



Research Article

Modified STATCOM control strategy for fault ride-through capability enhancement of grid-connected PV/wind hybrid power system during voltage sag

I. Hamdan¹ · Ahmed M. A. Ibrahim¹ · Omar NourEldeen¹

Received: 30 September 2019 / Accepted: 3 February 2020 / Published online: 7 February 2020
© Springer Nature Switzerland AG 2020

Abstract

This paper proposes the employment of Static Synchronous Compensator (STATCOM) in reactive power compensation to enhance the Fault Ride-Through (FRT) capability and improve the dynamic performance of a grid-connected PV/wind hybrid power system during the transient grid disturbances. The hybrid power system consisting of 9 MW Doubly Fed Induction Generator (DFIG)-based wind farm and 1 MW PV station is integrated with 100 MVAR STATCOM at the Point of Common Coupling (PCC) bus. The dynamic performance of the PV/wind hybrid power system with the proposed STATCOM controller is analyzed and compared with another FRT control strategy during a grid voltage sag. The FRT control strategy is based on the injection of reactive power from the hybrid system to enhance the FRT capability during the grid faults, and also activation of the outer crowbar protection system to protect the DFIG. On the other hand, the proposed STATCOM controller adjusts the PCC bus voltage during the grid disturbances by dynamically controlling the amount of reactive power injected to or absorbed from the electrical grid. Modeling and simulation of the proposed hybrid power system have been implemented using MATLAB/SIMULINK software. The effectiveness of both the proposed STATCOM controller and the FRT control strategy is evaluated during a 50% grid voltage sag. The simulation results illustrate that the STATCOM controller decreases significantly the level of voltage drop during the voltage sag, maintains the injected active power from the PV station at its rated value, and protects effectively the PV DC-link voltage from overvoltage. Moreover, when the STATCOM controller is employed, the injected active power from the wind farm is improved considerably and the oscillations of the DFIG rotor speed are reduced efficiently during the fault. Furthermore, the comparison confirms the superior dynamic performance of the STATCOM controller in enhancement the FRT capability as compared with the FRT control strategy.

Keywords PV · Wind · Hybrid system · STATCOM controller · FRT capability · Voltage sag

List of symbols

I_{pv}, V_{pv}	Output current and output voltage of the PV panel	T, q	PV cell temperature and the electron charge (1.602×10^{-19} C)
I_{ph}, I_o	Photocurrent generated by light and reverse saturation current through the diode	d, q	Subscribe d–q axis components in the synchronously rotating reference frame
R_s, R_{sh}	Series resistance and shunt resistance	V_{d-inv}, V_{q-inv}	d–q axis components of inverter voltage in the synchronously rotating reference frame
n, k	Ideality factor of the cell and the Boltzmann constant (1.38×10^{-23} J/K)	V_{dr}, V_{dq}	d–q axis components of grid voltage in the synchronously rotating reference frame

✉ Omar NourEldeen, omar_nourEldeen@svu.edu.eg | ¹Electrical Engineering Department, Faculty of Engineering, South Valley University, Qena 83523, Egypt.



ω_e	Rotation speed of the d–q synchronous reference frame with respect to the stationary axis
I_{d^*}, I_{q^*}	d–q axis components of inverter current in the synchronously rotating reference frame
R_{fi}, L_f	Resistance and inductance of the PV station filter
V_{dc1}, V_{dc1-f}	The DC-link voltage before and during the grid voltage sag
V_{fi}, I_g	RMS value of phase grid voltage during voltage sag and injected current from PV station
$C_1, \Delta t$	PV DC-link capacitor and duration of grid voltage sag
P_{mech}, P_e	Mechanical power of the wind turbine and the electrical power of the DFIG
V_w, C_p	The wind velocity and performance coefficient of the wind turbine
λ, β	Tip speed ratio of the rotor blade and the blade pitch angle
ρ, A_t	Air density and the area swept out by turbine blades
H_{gr}, δ, ω_s	Inertia constant, rotor angle, and synchronous speed of the DFIG
s, r	Denote the stator and rotor windings, respectively
V, i, λ, p	Subscribe voltage, current, flux linkage and number of pole pairs, respectively
R, L, M_{sr}	Resistance, self-inductance and mutual inductance of stator and rotor windings
ω_s, ω_r	Stator electrical angular speed and rotor mechanical angular speed
$V_{s^*}, V_{s-o^*}, \delta_s$	Fault-on and pre-fault stator voltage, and damping coefficient
i_{msr}, σ_s	Stator magnetizing current and stator leakage factor
i_{dgr}, i_{qg}	d–q axis components of the GSC current
V_{dc2}, C_2	DC-bus voltage and DC-bus capacitor
m, i_{orr}, L_{choke}	Stator modulation factor, DC-Bus current of RSC and inductance of DFIG filter
V_{gr}, V_{st}	Grid voltage and STATCOM voltage
α	Phase angle between STATCOM voltage and grid voltage
X_{tr}	Leakage reactance of coupling transformer between VSI and the grid

1 Introduction

Nowadays, the continuous growth of the electrical energy demand and the quick depletion of conventional energy resources have necessitated an imperative search for renewable energy resources as alternative energy sources.

Of the many renewable energy sources, PV energy and wind energy have been considered as the most promising sources toward meeting the permanent increase of the energy demand. The penetration level of the PV systems is currently significant and its usage is expected to increase globally due to the declined PV cell price and advanced power electronics technology. Also, wind energy is considered to be the most vital and promising renewable energy resource since being clean, global and can be harvested with large power capacity. However, wind energy and PV energy are not completely trustworthy and have some disadvantages such as they are unpredicted in nature and immensely depend on the variations of the environmental conditions such as solar irradiation and wind speed. Hence, the combination of PV energy and wind energy as a PV/wind hybrid generating power system can mitigate their individual variations, increase overall output energy, and inject more reliable power with greater quality into the electrical grid [1]. On the other hand, the increased penetration of the grid-connected PV/wind hybrid power systems has raised several concerns related to its dynamic performance during the grid voltage sag and the transient grid faults [2]. Recently, the national grid codes require that all grid-connected generation power plants (PV stations and wind farms) should have the capability of FRT in order to enhance its dynamic behavior during the grid faults. The FRT capability means that all generation power systems must remain connected to the electrical network during the transient grid faults and simultaneously inject reactive power to support the grid voltage, and also immediately resume the generated active power after fault clearance [3, 4].

Nowadays, several literatures have been carried out in the area of FRT capability enhancement for grid-connected generation power systems during the grid disturbances [5–7]. Among them, Al-Shetwi [5], presented a comprehensive review of several FRT strategies and controllers for grid-connected PV power plants under the grid fault conditions. In [8], the paper introduced a comprehensive Low Voltage Ride-Through (LVRT) capability control strategy for a single-stage inverter-based grid-connected PV power station. The employed control system ensures the reactive power support through the reactive current injection according to the standards grid codes requirements as soon as the grid voltage sag is detected. Also, the proposed control strategy eliminates the problems related to ac over-current and dc-link over-voltage that may cause disconnection or damage to the inverter under the grid faults. Also, Joshi [9], implemented adaptive control strategies in 100 kW grid-connected PV power plants to control active and reactive power during normal and abnormal grid conditions. Moreover, with respect to the

detection of voltage sag in the grid-connected PV power stations for LVRT capability control, two automatic fault detection methods are addressed in [10]. These methods are the Root Mean Square (RMS) that based d - q components of the grid voltage and the positive sequence voltage. These approaches are utilized to determine the voltage sag depth in order to regulate the required reactive current to be injected according to the LVRT grid codes requirements.

Furthermore, Hossain [6], proposed three nonlinear controllers to generate the appropriate resistance of Variable Resistive Fault current Limiter (VR-FCL) in order to enhance the transient stability of a large-scale grid-connected hybrid power system. The hybrid power system consisting of 50 MW PV plant, 60 MW DFIG-based wind farm, and 100 MVA synchronous generator. The effectiveness of the proposed control strategies in augmentation of the dynamic stability of the hybrid power system has been evaluated during symmetrical and unsymmetrical faults in the grid. In [7], the paper proposed an efficient control strategy to enhance the FRT capability of a hybrid power system consisting of 1 MW PV station and 9 MW DFIG-based wind farm during balanced and unbalanced grid faults. The proposed FRT control strategy based on modification of the control scheme so that inject reactive power during the faults and activation of the outer crowbar protection system to protect the DFIG.

Today, Flexible AC Transmission Systems (FACTS) devices like STATCOM, SVC, and UPFC can be employed for ensuring the power quality and the FRT capability of the grid-connected renewable energy sources and the microgrids. Several studies have recommended the employment of STATCOM to improve the FRT capability and mitigate voltage fluctuations during the grid disturbances [11–16]. Among them, Hemeida [15], presented a comprehensive comparison between STATCOM and SVC for stability improvement of a grid-connected wind farm during a three-line-to-ground (3LG) fault. In [17], the paper proposed a fuzzy controller-based SVC to enhance the voltage stability and LVRT capability a grid-integrated wind farm. Also, Döşoğlu [16], discussed the impact of STATCOM on FRT capability enhancement of DFIG-based wind farm during 3LG fault and double-line-to-ground (2LG) fault. Ahsan [11], discussed the impact of the integration between STATCOM and 12 MW wind farm-based Squirrel Cage Induction Generator (SCIG) during normal and abnormal conditions. In [12], the paper proposed a supercapacitor energy storage system interfaced through STATCOM to support the dynamic performance of the DFIG wind generation system during symmetrical 3LG fault. Noureldeen [13], suggested the utilization of STATCOM and supercapacitor to achieve constant active and reactive power from 200 MW wind farm during an extreme gust.

Furthermore, regarding multi-machine power systems, Movahedi [14], discussed the effects of three FACTS controllers on the transient stability of a multi-machine power system consisting of 120 MW PV plant and 200 MW wind farm based on DFIG. In addition, Zhou [18], investigated the employment of reinforcement learning controllers in conjunction with Convertible Static Compensator (CSC) to enhance the LVRT capability of a hybrid power system. The hybrid power system under study consists of two synchronous generators and one DFIG based wind farm. Furthermore, Jamil [19], explored the potential impact of STATCOM to improve the power transfer quality in a grid-tied PV-wind energy hybrid system during the presence of variable loading conditions.

However, so far, most previous studies have focused on FRT capability improvement of single renewable energy source connected to the electrical grid. No large-scale attempts have yet been made for FRT capability enhancement of large-scale grid-connected hybrid power systems, where more than one renewable energy source is employed. Therefore, the main objective of this study is to employ the STATCOM controller to enhance the FRT capability and support the dynamic performance of a grid-connected PV/wind hybrid power system during the transient grid faults. The hybrid power system consisting of 9 MW DFIG-based wind farm and 1 MW PV station is integrated with 100 MVAR STATCOM through the PCC bus. The dynamic performance of the PV/wind hybrid power system with the proposed STATCOM controller is analyzed and compared with another FRT control strategy during a grid voltage sag. The FRT control strategy is based on injection of reactive power from the hybrid system to enhance the FRT capability during the grid faults, and also activation of the outer crowbar protection system to protect the DFIG. On the other hand, the proposed STATCOM controller adjusts the PCC bus voltage during the grid disturbances by dynamically controlling the amount of reactive power injected to or absorbed from the electrical grid. The effectiveness of both the proposed STATCOM controller and the FRT control strategy is evaluated during a three-phase grid voltage sag of 50%.

2 Proposed hybrid power system with STATCOM

The proposed hybrid power system consists of 9 MW DFIG-based wind farm and 1 MW PV station which is integrated with 100 MVAR STATCOM at the PCC bus as illustrated in Fig. 1. The generated power from the PV/wind hybrid system is injected into the grid via 1 km double circuit transmission lines and 25/120 kV Δ/Y step-up transformer. The detailed specifications of the

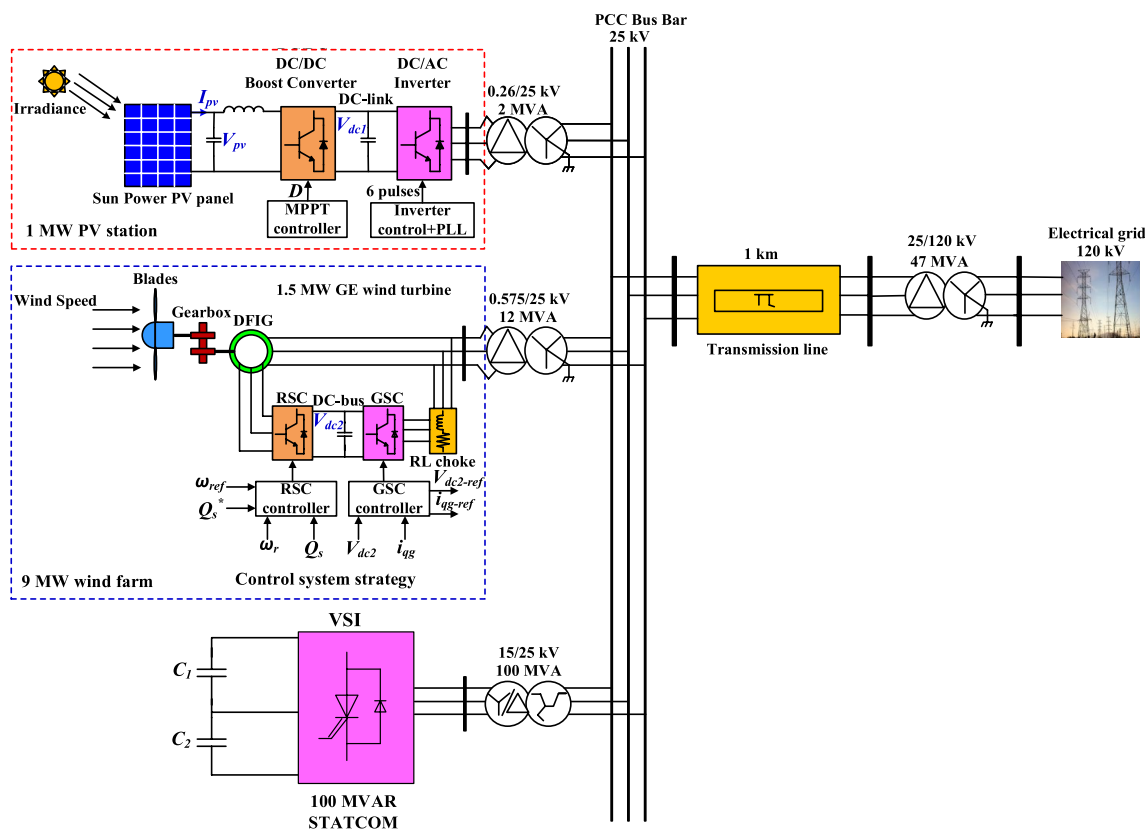


Fig. 1 Configuration of the proposed PV/wind hybrid power system with STATCOM

proposed hybrid power system and the STATCOM parameters are listed in Table 1. The PV station consists of 660 parallel-connected PV strings, each PV string formed by 5 PV panels connected in series to achieve the rated power of PV station (1 MW). Moreover, the PV station is equipped with a DC/DC boost converter to extract the optimum power during the change of solar radiation and it is synchronized with the grid through three-phase DC/AC inverter [6, 20].

On the other hand, the 9 MW wind farm consists of six variable-speed wind turbines from 1.5 MW General Electric (GE) wind turbine type [21]. Each wind turbine is equipped with DFIG including the Rotor Side Converter (RSC) to capture the maximum power during the variation of wind speed and the Grid Side Converter (GSC) to regulate the exchanged reactive power with the grid. Modeling and simulation of the wind farm have been implemented using SimPowerSystems toolbox in MATLAB/SIMULINK library. Moreover, as shown in Fig. 1, a typical 100 MVAR STATCOM is linked with the hybrid power system through the PCC bus to enhance the FRT capability and improves its dynamic performance during and after the grid disturbances. The main objective of the STATCOM controller is to regulate the PCC bus voltage during the grid voltage sag

by dynamically controlling the amount of reactive power injected to or absorbed from the electrical grid.

2.1 PV station configuration

2.1.1 PV system model

The implemented PV Station consists of 5 PV modules electrically connected in series to form a PV string and a total of 660 PV strings that are connected in parallel to reach the rated power (1 MW). SunPower SPR-305-WHT PV panel with a maximum power of 305.23 W is employed for this work [22]. Figure 2 shows the equivalent circuit of the PV system and the corresponding Current–Voltage (I–V) characteristics can be expressed as follows [23]:

$$I_{pv} = I_{ph} - I_d - I_{sh} = I_{ph} - I_o \left[\exp\left(\frac{V_{pv} + I_{pv}R_s}{a}\right) - 1 \right] - \frac{V_{pv} + I_{pv}R_s}{R_{sh}} \tag{1}$$

$$a = \frac{nkT}{q} \tag{2}$$

Table 1 Design specifications of the proposed hybrid power system and STATCOM parameters

<i>PV station parameters</i>	
Rated power of PV station	1 MW
Panel type	SunPower SPR-305-WHT
Rated power of PV panel	305.23 W
Number of parallel-connected PV strings	660
Number of series-connected PV panels per string	5
Standard Test Conditions (STC)	$G_{stc} = 1000 \text{ W/m}^2, T_{stc} = 25 \text{ }^\circ\text{C}$
Open-circuit voltage of PV panel	64.2 V
Short-circuit current of PV module	5.96 A
Nominal DC-link voltage	500 V
Power factor of the DC/AC Inverter	Unity
<i>Wind farm parameters</i>	
Rated power of wind farm (P_{wind})	9 MW
Wind turbine type	General Electric GE
Rated power of wind turbine	1.5 MW
Cut-in wind speed	3.5 m/s
Rated wind speed	11.5 m/s
Cut-out wind speed	20 m/s
Max DFIG rotor speed	1500 rev/min
Generator type	DFIG
Stator voltage	575 V
Frequency	60 Hz
Rated DC-bus voltage (V_{dc2})	1150 V
Stator resistance (R_s)	0.023 p.u
Rotor resistance (R_r)	0.016 p.u
Coefficient ($C_1 - C_6$)	[0.1576, 116, 0.4, 5, 21, 0.0068]
<i>STATCOM parameters</i>	
Rated power of STATCOM	100 MVAR
Rated frequency	60 Hz
Number of zigzag phase-shifting transformer	4
Primary voltage (zigzag connection)	25/4 kV
Secondary voltage (wye or delta connection)	15 kV
Eq. capacitance	2000 μF
Resistance of zigzag windings	0.05/30 p.u
Inductance of zigzag windings	0.05 p.u
Magnetizing resistance	500 p.u
Magnetizing inductance	500 p.u
<i>Grid parameters</i>	
Rated voltage	120 kV
Frequency	60 Hz
S.C level	1000 MVA
X/R	8

2.1.2 Inverter control strategy

The PV station is provided with the DC/DC boost converter to extract the maximum power during the variation of solar irradiance and integrated with the PCC bus through 3-level, 3-phase Pulse Width Modulation (PWM) inverter. The control strategy of the DC/AC inverter is

illustrated in Fig. 3. Voltage-Oriented Control (VOC) strategy is applied to adjust the DC-link voltage at a constant value and control the injected reactive power to the electrical grid. The inverter voltage in the d-q synchronous rotating reference frame can be described as follows [24, 25]:

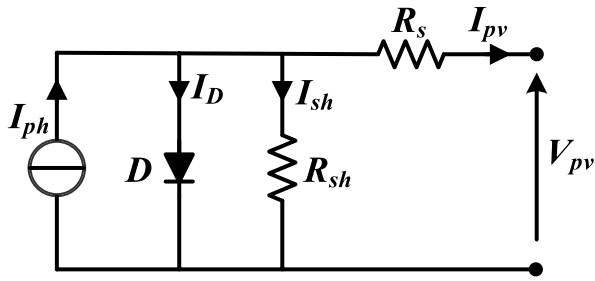


Fig. 2 Equivalent circuit of the PV system

$$V_{d_inv} = V_d + R_f I_d + L_f \frac{dI_d}{dt} - \omega_e L_f I_q \tag{3}$$

$$V_{q_inv} = V_q + R_f I_q + L_f \frac{dI_q}{dt} + \omega_e L_f I_d \tag{4}$$

The main parts of the DC/AC inverter controller are Phase Locked Loop (PLL), DC-link voltage controller, and current controller. Figure 3a shows the block diagram of the Phase Locked Loop (PLL). The main objective of the PLL is to generate the grid voltage angle (θ_{PLL}) that utilized for abc/d-q transformation and to synchronize the inverter output voltage (V_{abc_inv}) with the PCC bus voltage and the grid current [26, 27].

Moreover, the main task of the DC-link voltage controller is to maintain the voltage of DC-link at a specified constant value (500 V). As shown in Fig. 3b, the actual DC-link voltage (V_{dc1}) is compared with the reference value (V_{dc1_ref}) and the difference is applied to PI-controller to adjust the voltage at 500 V. Then, the output current of the voltage controller is utilized as reference d-axis component of inverter current (I_{d_ref}) for the inner current controller. During the steady-state operation, the DC power generated from the PV panels (P_{pv}) is the same as the AC power injected into the grid (P_{g_pv}).

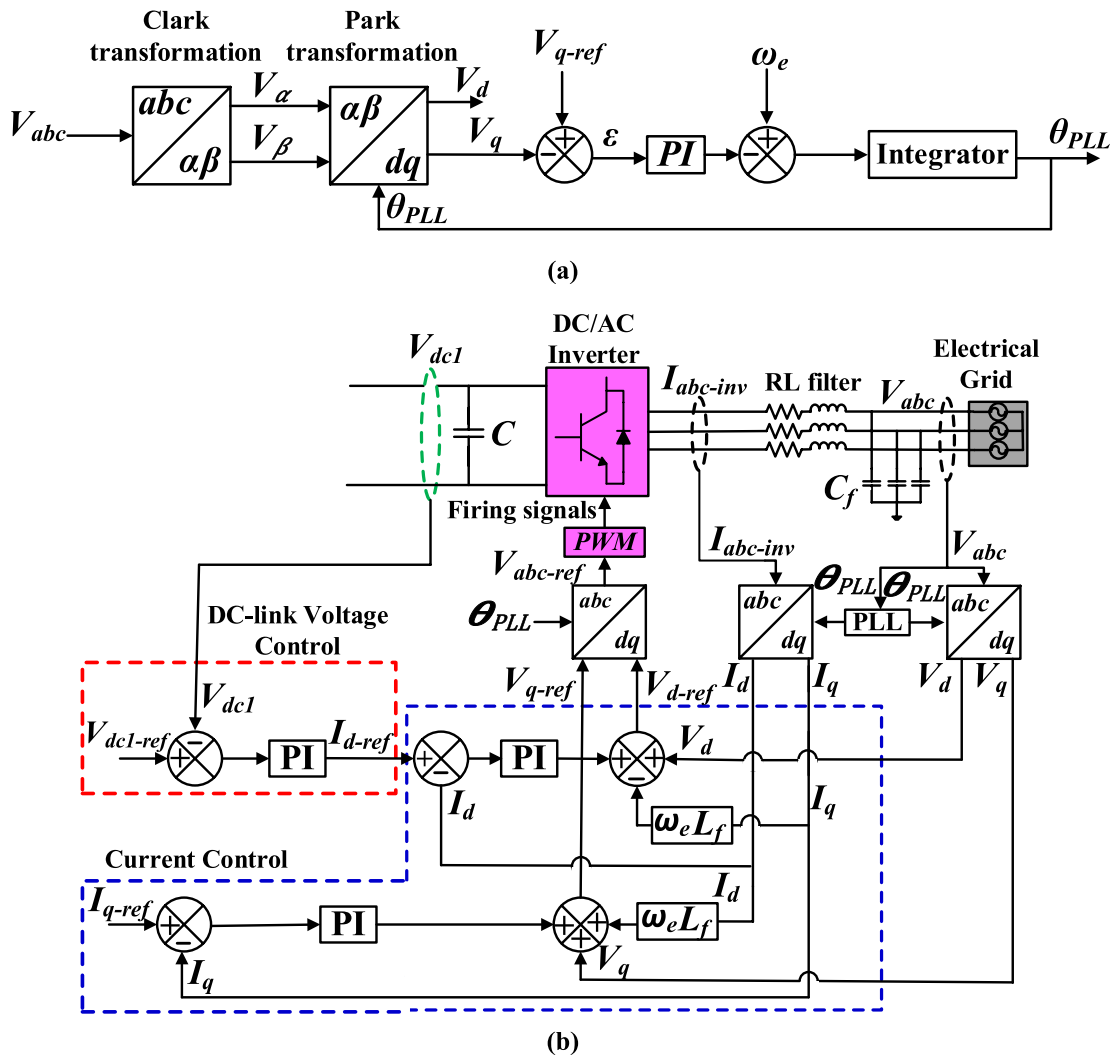


Fig. 3 a Block diagram of the PLL; b control strategy of the DC/AC inverter

Thus, the power balance sustains the V_{dc1} constant at its rated value (500 V). However, when a voltage sag occurs in the electrical grid, the voltage drop at the PCC bus reduces the injected PV station power into the grid from $P_{g,pv}$ to $P_{g,f}$. Meanwhile, the MPPT technique implemented on the DC/DC boost converter continues to extract the maximum power from the PV modules. Therefore, the power difference between the P_{pv} and the $P_{g,f}$ generates a severe increase in the DC-link voltage that can be expressed mathematically as [28, 29]:

$$(P_{pv} - P_{g,f})\Delta t = \frac{1}{2}C_1(V_{dc1_f}^2 - V_{dc1}^2) \tag{5}$$

$$V_{dc1_f} = \sqrt{\frac{2(P_{pv} - 3V_f I_g)\Delta t}{C_1} + V_{dc1}^2} \tag{6}$$

It can be observed from Eq. (6) that the increase of DC-link voltage during the grid voltage sag depends on the magnitude of voltage drop and the fault duration. Furthermore, the current control loop utilizes the I_{d-ref} to maintain the DC-link voltage constant at 500 V, while the reference q-axis current of inverter voltage (I_{q-ref}) is set to zero to maintain the PV station at unity power factor. Then, the I_{d-ref} and the I_{q-ref} are compared with the d-q axis components of the inverter current (I_d, I_q) and the errors are passed through PI-controllers to create the reference d-q axis components of inverter voltage (V_{d-ref}, V_{q-ref}). Finally, the V_{d-ref} and the V_{q-ref} are converted into reference three-phase voltage ($V_{abc-ref}$) that compared with the triangular carrier waveform of fixed switching frequency to generate the switching pulses for IGBTs switches of the inverter [30].

2.2 Wind farm configuration

The implemented wind farm consists of six variable-speed wind turbines from 1.5 MW General Electric (GE) type [21]. Each wind turbine is provided with the DFIG including the RSC controller to capture the peak power during the wind speed variation and the GSC controller to regulate the exchanged reactive power with the grid. Also, the wind farm is integrated with the main PCC bus through 0.575/25 kV Δ/Y step-up transformer to inject the generated power into the electrical grid. The mechanical power captured from the wind turbine is stated as follows [31, 32]:

$$P_{mech} = \frac{1}{2}C_p(\lambda, \beta)\rho A_t V_w^3 \tag{7}$$

$$C_p(\lambda, \beta) = C_1\left(\frac{C_2}{\lambda_i} - C_3\beta - C_4\right)e^{\left(-\frac{C_5}{\lambda_i}\right)} + C_6\lambda \tag{8}$$

$$\frac{1}{\lambda_i} = \frac{1}{\lambda + 0.08\beta} - \frac{0.035}{\beta^3 + 1} \tag{9}$$

During the grid voltage sag, all the generation sources inject fault current to the faulty node because of the severe voltage drop at that node, therefore the generated voltage and the injected active power of the wind farm are decreased. Thus, the DFIG incurs the instability and may lack the equilibrium state according to the swing equation as follows [33]:

$$\frac{2H_g}{\omega_s} \frac{d^2\delta}{dt^2} = P_{mech} - P_e \tag{10}$$

From Eq. (10), it is clear that during the grid voltage sag as the electrical output power from the DFIG becomes lower than the input mechanical power, the DFIG suffers from the instability due to the acceleration of the DFIG rotor.

2.2.1 DFIG model under the grid voltage sag

The two-axis fourth-order model of the DFIG in the synchronously rotating reference frame is employed to study the dynamic performance under the grid voltage sag. The flux linkage and voltage for the stator and rotor are described as follows [34]:

$$V_s = R_s i_s + j\omega_s \lambda_s + \frac{d\lambda_s}{dt} \tag{11}$$

$$V_r = R_r i_r + j(\omega_s - p\omega_r)\lambda_r + \frac{d\lambda_r}{dt} \tag{12}$$

$$\lambda_s = M_{sr} i_r + L_s i_s \tag{13}$$

$$\lambda_r = L_r i_r + M_{sr} i_s \tag{14}$$

During the normal operating conditions with constant stator voltage (V_s), the stator flux linkage (λ_s) remains almost constant, therefore the stator dynamics ($\frac{d\lambda_s}{dt}$) can be neglected. However, when three-phase voltage sag occurs, the stator voltage fluctuates and the λ_s decreases proportionally to the grid voltage. According to constant flux linkage principle, the value of λ_s divided into to stationary portion with respect to the stator (natural component) and a rotating portion at synchronous speed (forced component). The amplitude of the forced component is proportional to the maintaining voltage, while the natural component magnitude depends on the amplitude of voltage dip during fault and generates large Electromagnetic Force (EMF) in the rotor windings. The stator flux linkage and the rotor dynamics as referred to the rotor reference frame can be expressed as follows [34, 35]:

regulator loop after comparing the stator voltage (V_s) with the reference value (V_{ref}). Therefore, the DFIG injects reactive power to enhance the FRT capability of the wind farm and support its dynamic performance during the voltage sag. Then, the i_{dr-ref} and the i_{qr-ref} are compared with the d-q axis components of the measured rotor current (i_{dr} , i_{qr}) to create the reference d-q axis components of the rotor voltage (V_{d-ref} , V_{q-ref}), that can be stated mathematically as follows [37, 39, 40]:

$$V_{dr-ref} = V_{dr}^* - (\omega_e - \omega_r) \sigma_s L_r i_{qr} \tag{22}$$

$$V_{qr-ref} = V_{qr}^* + (\omega_e - \omega_r) \left(\frac{L_m^2}{L_s} i_{ms} + \sigma_s L_r i_{dr} \right) \tag{23}$$

2.2.3 Grid side converter (GSC) controller

The GSC controller is utilized to maintain the DC-bus voltage (V_{dc2}) constant irrespective of magnitude and direction of rotor power flow and regulate the reactive power exchanged with the grid. Voltage-Oriented Control (VOC) system is used to accomplish the decoupled control strategy of the GSC. Hence, the injected active power from the GSC (P_c) and the DC-bus voltage (V_{dc2}) is adjusted through i_{dg} , while the injected reactive power from the GSC (Q_c) is controlled by the i_{qg} as follows [41, 42]:

$$P_c = \frac{3}{2} (V_d i_{dg} + V_q i_{qg}) = \frac{3}{2} V_d i_{dg} \tag{24}$$

$$Q_c = \frac{3}{2} (V_q i_{dg} - V_d i_{qg}) = -\frac{3}{2} V_d i_{qg} \tag{25}$$

$$C_2 \frac{dV_{dc2}}{dt} = \frac{3m}{4\sqrt{2}} i_{dg} - i_{or} \tag{26}$$

Figure 5 illustrates the control strategy of the GSC. The GSC controller employs the d-axis component to keep the DC-bus voltage (V_{dc2}) constant at 1150 V irrespective of the magnitude and direction of the rotor power flow. Therefore, the reference d-axis component of the GSC current (i_{dg-ref}) is generated from comparing the reference DC-bus voltage ($V_{dc2-ref}$) with the measured value (V_{dc2}) and applying the difference to PI-controller.

On the other hand, the q-axis component (i_{qg}) is employed to control the exchanged reactive power with the electrical grid. During the normal operation conditions, the reference q-axis component of the GSC current (i_{qg-ref}) is determined at zero value to maintain the wind farm at unity power factor. Then, the i_{dg-ref} and the i_{qg-ref} are compared with the d-q axis components of measured GSC current (i_{dg} , i_{qg}) and the differences are applied to PI-controllers to create the reference d-q axis components of GSC voltage (V_{dg-ref} , V_{qg-ref}) that can be described as [41]:

$$V_{dg-ref} = -V_{dg}^* + \omega_e L_{choke} i_{qg} + V_d \tag{27}$$

$$V_{qg-ref} = -V_{qg}^* - \omega_e L_{choke} i_{dg} \tag{28}$$

2.3 STATCOM configuration and control strategy

A typical ± 100 MVAR STATCOM is connected to the electrical grid at the PCC bus as shown in Fig. 1. The main objective of the STATCOM controller is to regulate the PCC bus voltage by dynamically controlling the amount of reactive power injected to or absorbed from the grid. Figure 6 shows the equivalent circuit of the STATCOM.

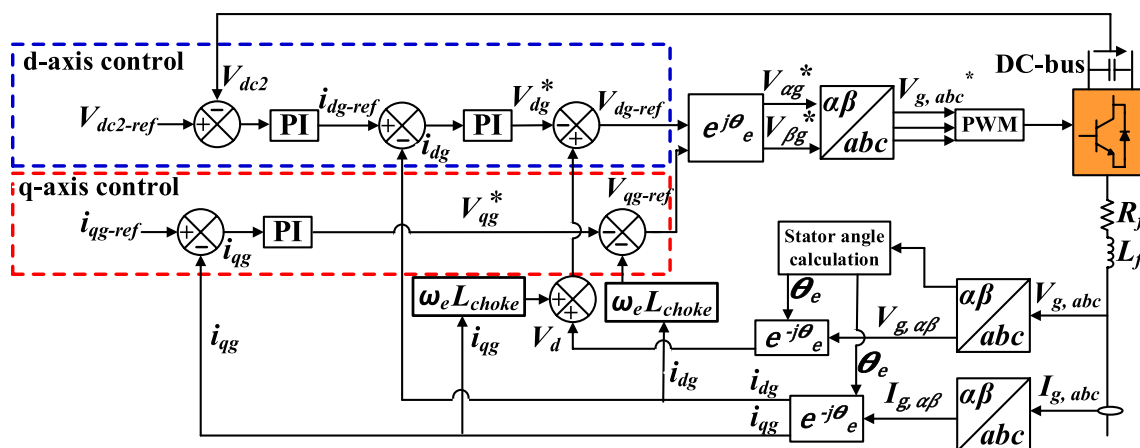


Fig. 5 Control scheme of the GSC

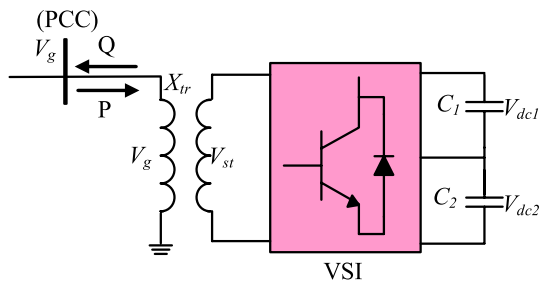


Fig. 6 Equivalent circuit of the STATCOM

It basically consists of Voltage Source Inverter (VSI) based on Gate Turn-Off thyristor (GTO) that generates AC voltage with less harmonics, coupling transformer between VSI and the grid, and DC-link capacitor which acts as a storage system for reactive power compensation. The active and reactive power transfer between the STATCOM and the electrical grid can be expressed mathematically as follows [13, 43]:

$$P = 3 \left(\frac{V_g V_{st}}{X_{tr}} \right) \sin(\alpha) \tag{29}$$

$$Q = 3 \left(\left(\frac{V_g V_{st}}{X_{tr}} \right) \cos(\alpha) - \frac{V_g^2}{X_{tr}} \right) \tag{30}$$

It can be seen that the active power flow is dominated by changing the phase angle between STATCOM voltage and grid voltage (α), while the STATCOM reactive power depends on the difference between the STATCOM voltage and grid voltage. It is clear also from Eq. (30) that when a grid voltage sag occurs and the PCC bus voltage (V_g) becomes less than the STATCOM voltage (V_{st}), the STATCOM acts as a capacitor injecting reactive power to the grid. On the reverse, when the PCC bus voltage is greater than the STATCOM voltage, the STATCOM operates as an inductor absorbing reactive power from the grid [43].

2.3.1 Voltage sag detection

The voltage sag detection method is a strategy that detects the occurrence of sudden disturbances in the electrical grid such as the transient faults and the voltage dips. In this paper, the voltage sag detection method is implemented using the peak value technique based on the orthogonal signal generator which employs the quarter period ($T/4$) delay structure. This strategy has many merits such as flexibility, fast response, ease in the implementation [44]. Figure 7 shows the voltage sag detection method using the peak value technique that can be expressed mathematically as follows:

$$V_m = \sqrt{V_g^2 + V_g'^2} = \sqrt{V_m^2 \sin^2(\omega t) + V_m^2 \cos^2(\omega t)} \tag{31}$$

Furthermore, the national grid codes as such as the E.ON Netz grid code proposed by Germany require that all grid-connected renewable energy generation sources should have the FRT capability during the grid voltage sag. The FRT capability means that all generation power plants (PV stations and wind farms) must remain connected to the electrical network during the transient grid faults and simultaneously inject reactive power to support the grid voltage, and also immediately resume the generated active power after fault clearance. Figure 8 illustrates the amount of required reactive current during the grid voltage sag according to the German grid code [45]. It is clear that when the magnitude of grid voltage sag is equal to 50% of the rated value, the amount of injected reactive current should be equal to 1 p.u.

2.3.2 STATCOM configuration

Figure 9 demonstrates the configuration of the 48-pulse STATCOM that employed to regulate the voltage at the PCC bus and enhance the FRT capability of the hybrid power system by injecting leading or lagging current to the grid. It comprises four 3-phase, 3-level GTO inverters coupled with four 3-phase phase-shifting transformers introducing a phase shift of $\pm 7.5^\circ$. In this configuration, the STATCOM DC-link is interconnected with the four inverters

Fig. 7 Voltage sag detection method using peak value technique

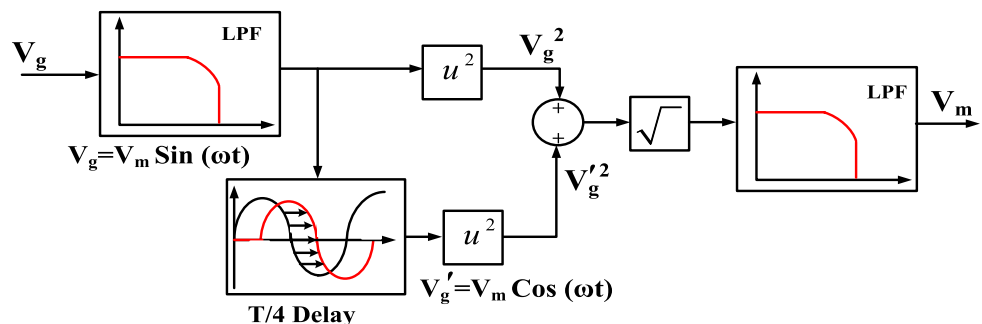


Fig. 8 Injected reactive current during the voltage sag according to the German grid code

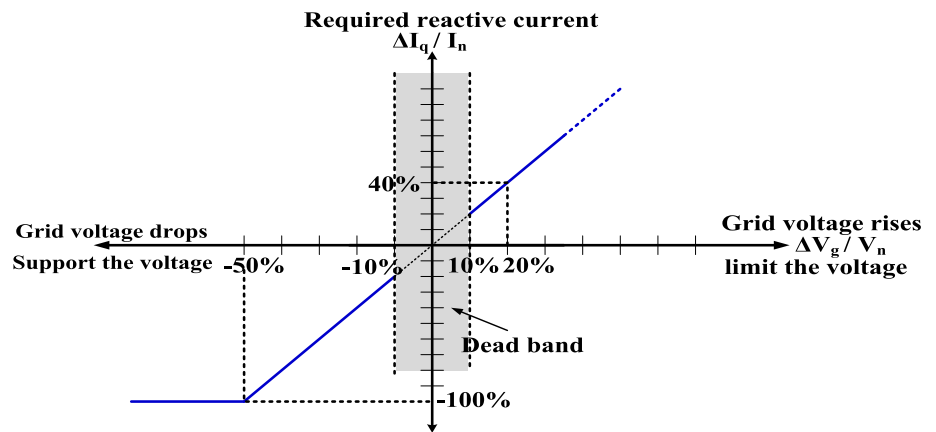
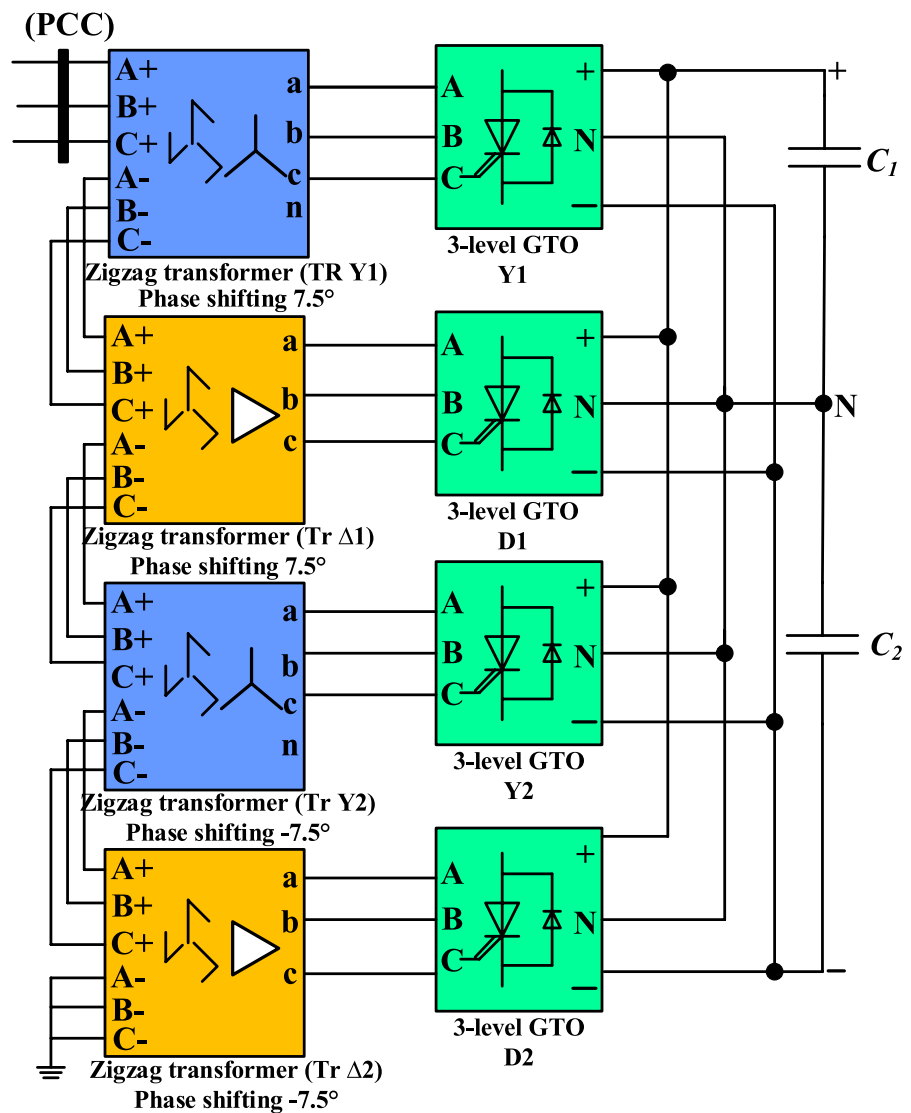


Fig. 9 Configuration of the ± 100 MVAR STATCOM based on 48-pulse GTO VSI



and the generated voltages from the inverters are supplied to the secondary windings of the zigzag phase-shifting transformers that linked in Δ or Y to neutralize all

odd harmonics [46]. In addition, the inverter's pulse patterns are phase-shifted and the primary windings of the transformers are connected in series so that the STATCOM

generates a 48-step voltage (V_{st}) approximating a sin wave. The main advantages of this configuration are the elimination of harmonic distortion in the STATCOM voltage and the prevention of problems related to power quality and system harmonic instability [47].

2.3.3 STATCOM control strategy

The control strategy of the STATCOM is implemented as illustrated in Fig. 10. It consists of the Phase Locked Loop (PLL) that generates the reference angle (θ_{PLL}) for abc/dq transformation and synchronizes the GTO thyristors pulses with the grid voltage. In the outer voltage regulator loop, the actual PCC bus voltage (V_g) is compared with the reference value (V_{ref}) and the difference is applied to the PI controller to generate the reference reactive current (I_{q-ref}). Then, the inner current regulation loop compares the injected or absorbed reactive current (I_q) with the reference value (I_{q-ref}) to produce the desired phase angle (α) which is the phase shift of the STATCOM voltage (V_{st}) with respect to the grid voltage (V_g) [48]. Also, the conduction angle of the 3-level inverters (σ) is fixed to 172.5° to minimize the 23rd and the 25th harmonics of generated voltage from the square-wave inverters. Moreover, to eliminate the non-characteristic harmonics, using the DC-link voltage regulator, the positive and negative voltages of the DC-link capacitor are forced to maintain equal by applying a slight offset ($\Delta\alpha$) on the conduction angles (σ) for the positive and negative half-cycles. Finally, the firing pulses generator utilizes the phase angle (α) from the current regulator and the output ($\omega.t$) from the PLL to generate the 48 pulses for the four GTO inverters [43, 47]. The STATCOM control strategy can be expressed mathematically as follows:

$$I_{q-ref} = (V_{ref} - V_g) \left(K_p + \frac{K_i}{s} \right) \tag{32}$$

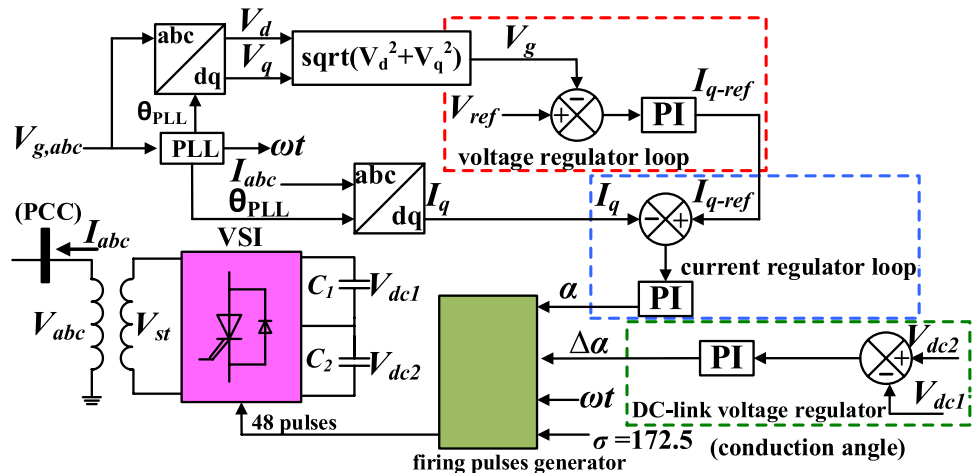
$$\alpha = (I_{q-ref} - I_q) \left(K_p + \frac{K_i}{s} \right) \tag{33}$$

$$\Delta\alpha = (V_{dc2} - V_{dc1}) \left(K_p + \frac{K_i}{s} \right) \tag{34}$$

3 Simulation results and discussion

The grid-connected PV/wind hybrid power system under study is shown in Fig. 1. During the normal operation conditions, the PV station is under the Standard Test Conditions (Irradiance (G) = 1000 W/m^2 and Temperature (T) = 25°C), and the wind farm is subjected to the rated wind speed (11.5 m/s). Therefore, during the steady-state operation, the injected active power from the hybrid power system is equal to 10 MW divided as 1 MW from the PV station and 9 MW from the wind farm. However, under low voltage fault conditions, the PCC bus voltage drops sharply and generally the injected active power into the grid decreases significantly. In this section, the dynamic performance of the hybrid power system with the proposed STATCOM controller shown in Fig. 10 is analyzed and compared with the proposed FRT control strategy in the literature [7]. The proposed FRT control strategy is based on the modification of the inverter and RSC controllers so that inject reactive power during the faults and also activation of the outer crowbar protection system to protect the DFIG [7]. The effectiveness of both the proposed FRT control strategy and the STATCOM controller is evaluated

Fig. 10 Control scheme of the STATCOM



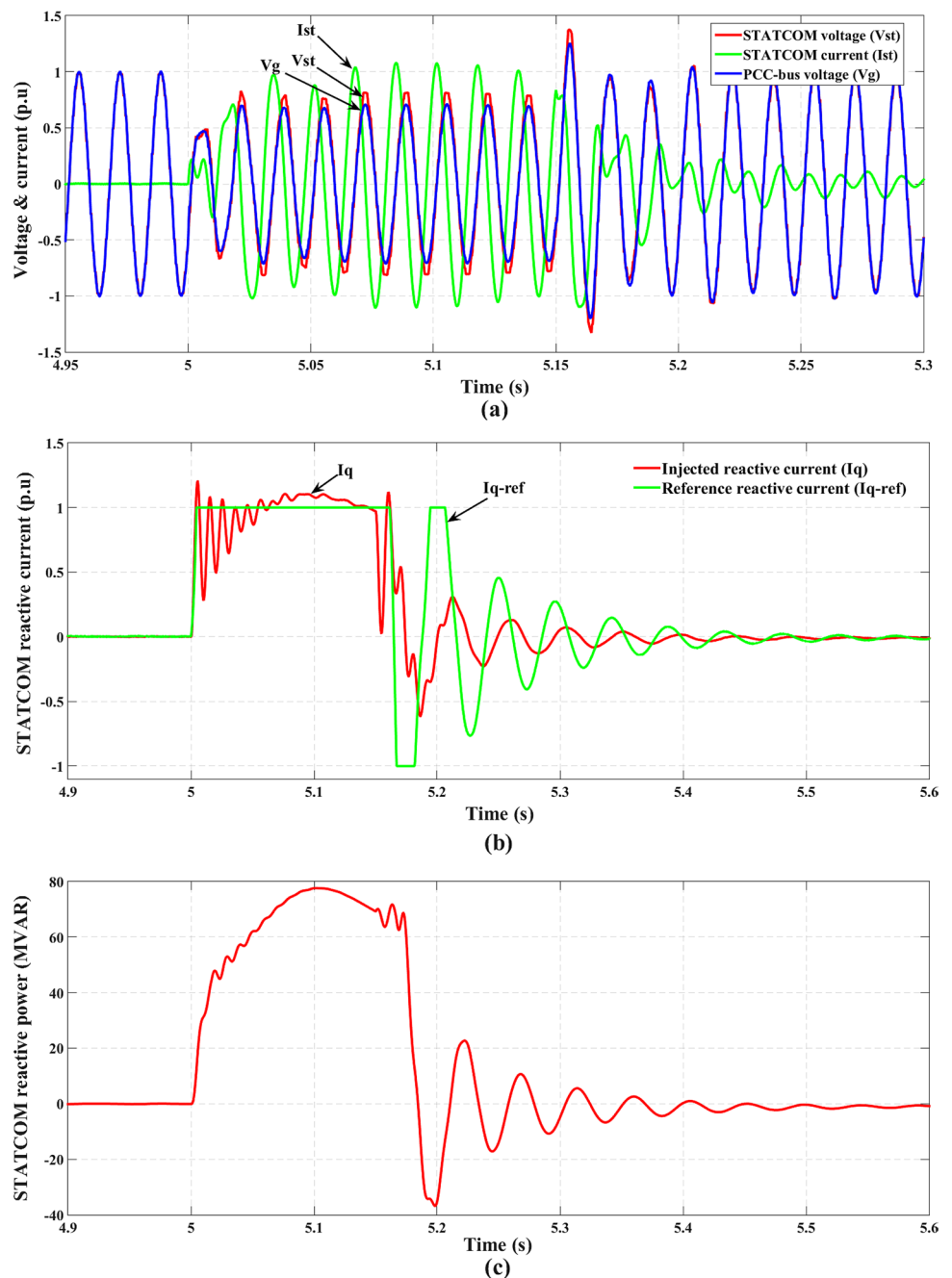
during a three-phase grid voltage sag of 50% occurring at $t=5$ s and lasting for 150 ms (9 cycles) [49].

3.1 Dynamic response of the STATCOM controller

In this subsection, the dynamic response of the STATCOM controller to the 50% three-phase grid voltage sag is investigated. Figure 11a illustrates the dynamic response of the STATCOM voltage and the STATCOM current to the fault. Since the STATCOM operates in capacitive mode during the voltage sag, the STATCOM voltage (V_{st}) is greater

than and in phase with the PCC bus voltage (V_g) and the STATCOM current (I_{st}) leads the STATCOM voltage by 90° ; the STATCOM is, therefore, generating reactive power. Figure 11b demonstrates that during the grid voltage sag, the injected reactive current from the STATCOM follows the required reactive current according to the German grid code. Since the magnitude of grid voltage sag is 50% of the rated value, the amount of injected reactive current is about 1 p.u. Figure 11c shows the STATCOM reactive power that injected according to the difference between the STATCOM voltage and the PCC bus voltage during the

Fig. 11 Response of the STATCOM controller to the 50% voltage sag **a** STATCOM voltage, STATCOM current, and PCC bus voltage; **b** STATCOM reactive current; **c** STATCOM reactive power



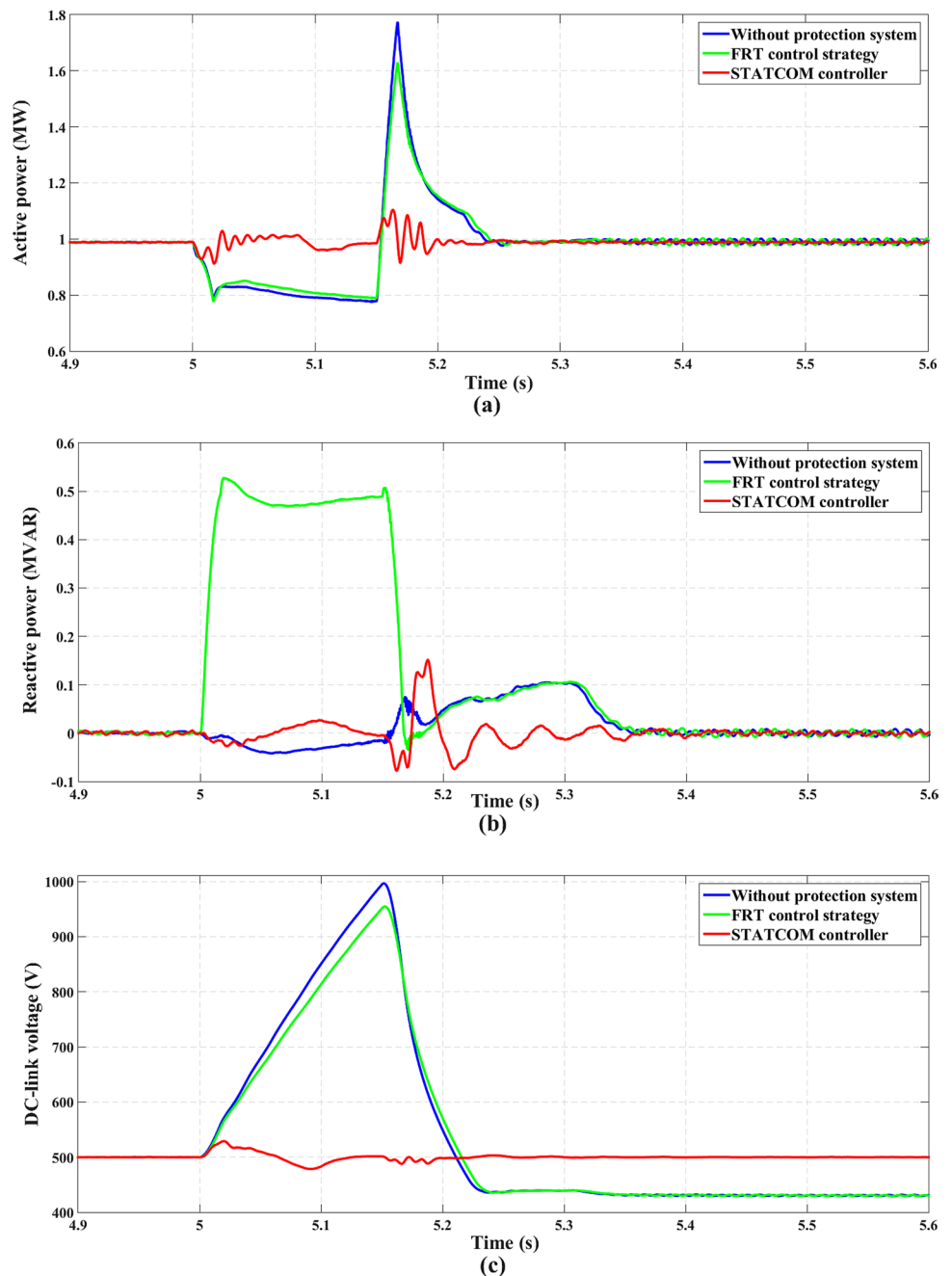
grid voltage dip. When the grid voltage sag occurs, the STATCOM controller reacts by generating a reactive power of 77.6 MVAR to increase the PCC bus voltage to 0.69 p.u as compared to 0.5 p.u when the STATCOM is not employed.

3.2 Dynamic performance of the PV station

Figure 12 compares the impact of both the STATCOM controller and the FRT control strategy on the dynamic performance of the PV station during the event of the 50% grid voltage sag. Figure 12a depicts the injected active power

from the PV station. During the steady-state operation, the PV station utilizes the MPPT technique to inject the maximum power of 1 MW into the PCC bus. However, during the grid voltage sag, when the proposed FRT control strategy in [7] is implemented, the PV station power increases slightly to 0.83 MW compared to 0.79 MW without any protection system. Also, after fault clearance, the overshoot of active power decreases by 0.15 MW with the FRT control strategy. On the other hand, when the STATCOM controller is employed, the injected active power maintains constant at its rated value (1 MW) during the voltage sag

Fig. 12 Dynamic performance of the PV station during 50% voltage sag **a** injected active power from the PV station; **b** injected reactive power from the PV station; **c** PV DC-link voltage



and its overshoot after fault clearance is eliminated. From Fig. 12b, it is clear that when the FRT control strategy is applied during the voltage sag, the PV station has to inject reactive power of 0.47 MVAR to enhance the FRT capability. However, with the STATCOM controller, the injected reactive power sustains at zero during and after the fault occurrence to keep the PV station at a unity power factor. Figure 12c illustrates the response of the PV DC-link voltage to the grid voltage sag. In both cases (1) without protection system, (2) with the FRT control strategy, the DC-link voltage increases drastically to 1000 V and 950 V, respectively because of the great difference between the extracted power from the PV station and the power injected into the grid. Moreover, after the voltage sag is cleared, the DC/AC inverter controller fails to retrieve the DC-link voltage to its rated value due to the severe voltage drop and the large overshoot of the DC-link voltage during the fault. In contrast, when the STATCOM controller is employed, the DC-link voltage successfully maintains constant at its reference value (500 V) during and after the fault occurrence.

3.3 Dynamic performance of the wind farm

The following results discuss the dynamic behavior of the wind farm under the 50% grid voltage sag. Figure 13a demonstrates the active power transmitted from the wind farm to the PCC bus. During the normal operation conditions, the MPPT technique is implemented on the RSC to extract the maximum power from the wind farm, so the injected active power is equal to the rated value (9 MW). However, when the grid voltage sag occurs, in the case with the FRT control strategy, the wind farm power rises to 6.1 MW compared to 5.5 MW without any protection system. But when the STATCOM control strategy is implemented, the injected active power from wind farm increases significantly to 7.4 MW during the fault and quickly returns back to its rated value after fault clearance. Figure 13b illustrates that when the STATCOM controller is utilized during the grid voltage sag, the injected reactive power from the wind farm increases slightly by 0.2 MVAR compared to without protection system and with the FRT control strategy. Figure 13c illustrates the response of the DC-bus voltage to the grid voltage sag. Compared to the cases without any protection system and with the STATCOM controller, the FRT control strategy reduces considerably the oscillations of the DC-bus voltage during and after the fault occurrence.

Figure 13d shows the variation of the mechanical torque of the wind turbine during the grid voltage dip. It is clear that in the case without any protection system, the mechanical torque during the grid fault drops sharply to 0.29 p.u compared to 0.38 p.u when the FRT control

strategy is applied. However, when the STATCOM controller is employed, the drop in the mechanical torque is decreased by 0.25 p.u compared to without protection system and it quickly returns back to its rated value (0.8 p.u) after the fault clearance. Figure 13e illustrates that without any protection system and with the FRT control strategy, the DFIG rotor speed oscillates severely to 1.27 p.u during the voltage sag. The oscillations of the rotor speed are due to the injected active power from the DFIG decreases significantly during the fault and the mechanical power of the wind turbine cannot be converted completely into electrical power. But when the STATCOM controller is used, the rotor speed oscillations are low and the time for reaching its pre-fault value (1.2 p.u) is quicker when the fault is cleared.

3.4 Dynamic performance of the PV/wind hybrid power system at the PCC bus

In this subsection, the dynamic performance of the hybrid power system at the PCC bus during the grid voltage sag is discussed. As can be seen from Fig. 14a, without the STATCOM control strategy, the PCC bus voltage decreases sharply to 0.5 p.u during the grid voltage dip. However, when the STATCOM controller is employed, the voltage raises significantly to 0.7 p.u. Figure 14b shows the injected active power from the hybrid power system. It is clear that when the STATCOM controller is utilized during the voltage sag, the active power increases considerably to 8.5 MW as compared to 6.3 MW without protection system and 6.9 MW with the FRT control strategy. Also, in the case with the STATCOM controller, the injected active power rapidly returns back to its rated value (10 MW) after the fault clearance. Figure 14c illustrates that when the STATCOM controller is employed, the injected reactive power at the PCC bus during the voltage sag is equal to about 78.11 MVAR so that the FRT capability and the dynamic performance of the hybrid system can be enhanced. From the previous results, it can be observed that the dynamic performance of the hybrid power system during the grid voltage sag is greatly improved with the proposed STATCOM controller when compared to the FRT control strategy in the literature [7].

4 Conclusions

In this paper, the STATCOM controller has been utilized in reactive power compensation to enhance the FRT capability and improve the dynamic performance of a grid-connected PV/wind hybrid power system during the transient grid faults. The hybrid power system consisting of 9 MW DFIG-based wind farm and 1 MW PV station is

Fig. 13 Dynamic performance of the wind farm during 50% voltage sag **a** injected active power from the wind farm; **b** injected reactive power from the wind farm; **c** DC-bus voltage; **d** mechanical torque of the wind turbine; **e** DFIG rotor speed

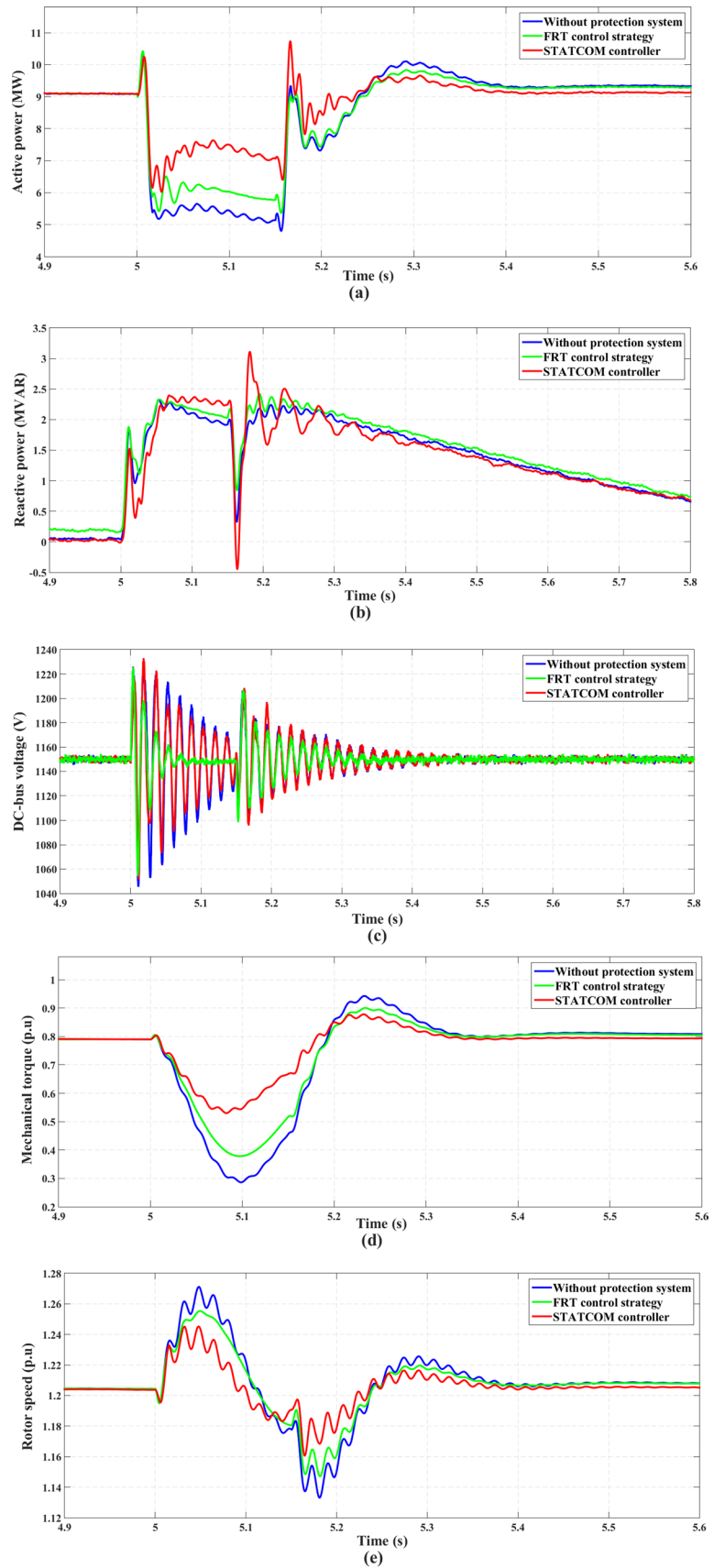
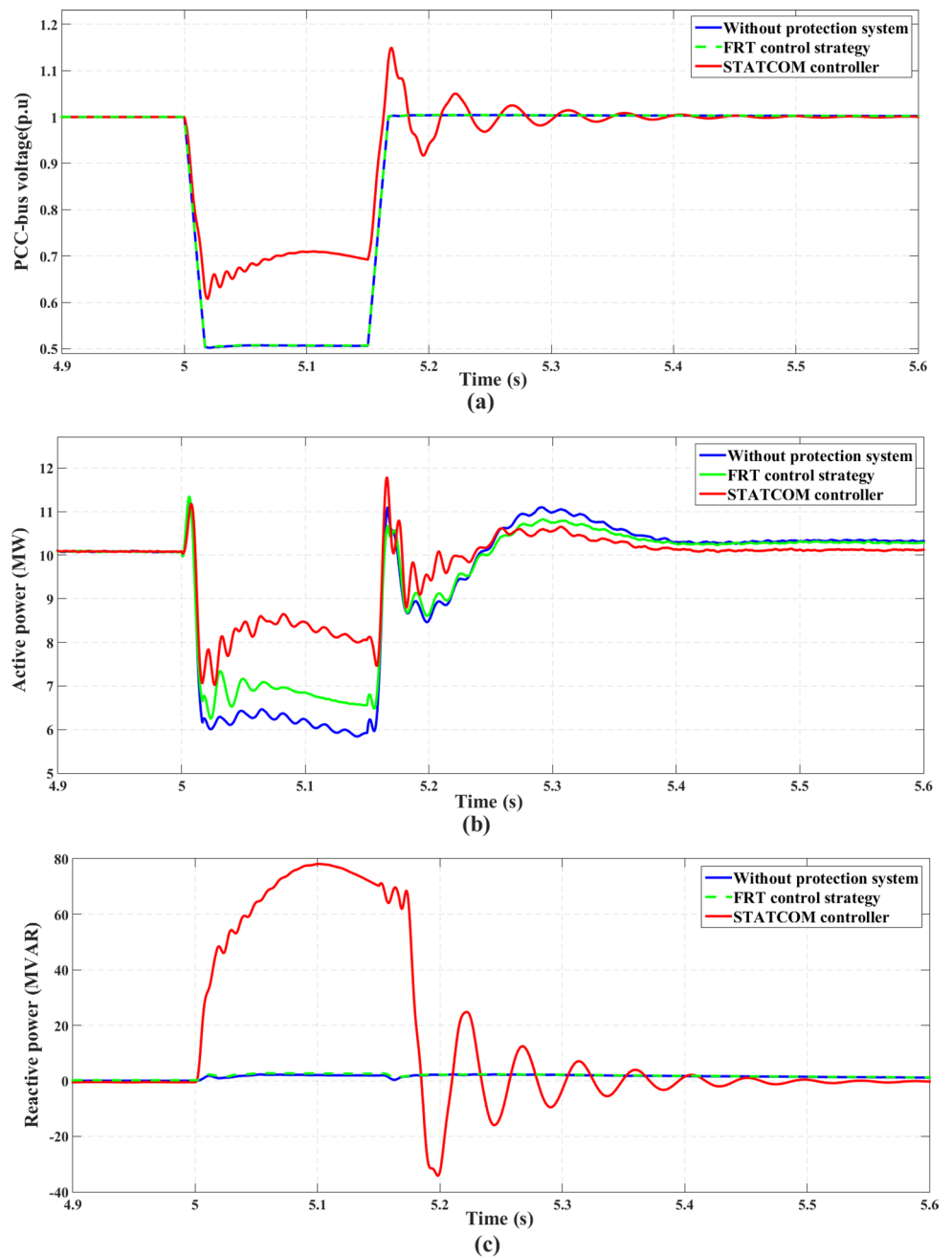


Fig. 14 Performance of PV/wind hybrid system at PCC bus during 50% voltage sag **a** terminal voltage at the PCC bus in p.u.; **b** injected active power from the PV/wind hybrid system at the PCC bus; **c** injected reactive power at the PCC bus



merged with 100 MVAR STATCOM through the main PCC bus. The dynamic performance of the hybrid power system with the proposed STATCOM controller is evaluated and compared with another FRT control strategy during a grid voltage dip. The FRT control strategy is based on injection of reactive power from the hybrid system to enhance the FRT capability during the grid faults, and also activation of the outer crowbar protection system to protect the DFIG. On the other hand, the proposed STATCOM controller regulates the PCC bus voltage during the grid disturbances by dynamically controlling the amount of reactive power

injected to or absorbed from the electrical network. The validity of both the proposed STATCOM controller and the FRT control strategy is verified during a 50% grid voltage sag for 150 ms. The simulation results have proved that the STATCOM controller raises significantly the PCC bus voltage during the grid voltage sag to 0.7 p.u. as compared to 0.5 p.u. without the STATCOM. Moreover, the STATCOM control strategy sustains effectively the PV station power at its rated value (1 MW) as compared to 0.83 MW with the FRT control strategy and 0.79 MW without any protection system. In addition, the STATCOM controller protects successfully the PV DC-link voltage from overshoot

by maintaining its rated value (500 V) as compared to the sharp increase to 1000 V and 950 V with the FRT strategy and without protection system, respectively.

On the other hand, when the STATCOM controller is employed during the fault, the wind farm power is improved considerably to 7.4 MW as compared to 6.1 MW with the FRT control strategy and 5.5 MW without any protection system. Also, the STATCOM control system reduces efficiently the oscillations of the DFIG rotor speed and decreases the drop in the mechanical torque of the wind turbine during the fault. The comparison illustrates that the dynamic performance of the hybrid power system during the grid voltage sag is greatly improved with the proposed STATCOM controller when compared to the FRT control strategy.

Compliance with ethical standards

Conflict of interest The authors declare that they have no conflict of interest.

References

- Sawle Y, Gupta S, Bohre AK (2016) PV-wind hybrid system: a review with case study. *Cogent Eng* 3:1–31
- Kumar M, Sandhu K, Kumar A (2014) Simulation analysis and THD measurements of integrated PV and wind as hybrid system connected to grid. In: IEEE 6th India International Conference on Power Electronics (IICPE), pp 1–6
- Sulla F (2012) Fault behavior of wind turbines. Ph.D. Thesis, Dept. Measurement Technology and Electrical Eng, Lund University
- Kasem A, El-Saadany E, El-Tamaly H, Wahab M (2008) An improved fault ride-through strategy for doubly fed induction generator-based wind turbines. *IET Renew Power Gener* 2:201–214
- Al-Shetwi AQ, Sujod MZ, Blaabjerg F, Yang Y (2019) Fault ride-through control of grid-connected photovoltaic power plants: a review. *Sol Energy* 180:340–350
- Hossain MK, Ali MH (2015) Transient stability augmentation of PV/DFIG/SG-based hybrid power system by nonlinear control-based variable resistive FCL. *IEEE Trans Sustain Energy* 6:1638–1649
- Noureldeen O, Ibrahim AM (2017) Low-voltage ride-through capability enhancement of a grid-connected photovoltaic/wind hybrid power system. In: 2017 nineteenth international Middle East Power Systems Conference (MEPCON), pp 786–795
- Al-Shetwi AQ, Sujod MZ, Blaabjerg F (2018) Low voltage ride-through capability control for single-stage inverter-based grid-connected photovoltaic power plant. *Sol Energy* 159:665–681
- Joshi V, Mehta B, Joshi S (2020) Active and reactive power control of photovoltaic power plant under normal and abnormal grid conditions. In: *Advances in control systems and its infrastructure*, ed. Springer, pp 109–122
- Al-Shetwi AQ, Sujod MZ (2019) Voltage sag detection in grid-connected photovoltaic power plant for low voltage ride-through control. *Recent Adv Electr Electron Eng (Formerly Recent Patents on Electrical & Electronic Engineering)* 12:384–392
- Ahsan S, Siddiqui A (2016) Dynamic compensation of real and reactive power in wind farms using STATCOM. *Perspect Sci* 8:519–521
- Rahim A, Nowicki E (2012) Supercapacitor energy storage system for fault ride-through of a DFIG wind generation system. *Energy Convers Manag* 59:96–102
- Noureldeen O, Youssef MM, Hassanin B (2019) Stability improvement of 200 MW Gabal El-Zayt wind farm connected to electrical grid using supercapacitor and static synchronous compensator during extreme gust. *SN Appl Sci* 1:331
- Movahedi A, Niasar AH, Gharehpetian G (2019) Designing SSSC, TCSC, and STATCOM controllers using AVURPSO, GSA, and GA for transient stability improvement of a multi-machine power system with PV and wind farms. *Int J Electr Power Energy Syst* 106:455–466
- Hemeida M, Rezk H, Hamada MM (2018) A comprehensive comparison of STATCOM versus SVC-based fuzzy controller for stability improvement of wind farm connected to multi-machine power system. *Electr Eng* 100:935–951
- Döşoğlu MK, Arsoy AB, Güvenç U (2017) Application of STATCOM-supercapacitor for low-voltage ride-through capability in DFIG-based wind farm. *Neural Comput Appl* 28:2665–2674
- Rezaie H, Kazemi-Rahbar MH (2019) Enhancing voltage stability and LVRT capability of a wind-integrated power system using a fuzzy-based SVC. *Eng Sci Technol Int J* 22:828–839
- Zhou L, Swain A, Ukil A (2019) Reinforcement learning controllers for enhancement of low voltage ride through capability in hybrid power systems. *IEEE Trans Ind Inform.* <https://doi.org/10.1109/TII.2019.2956509>
- Jamil E, Hameed S, Jamil B (2019) Power quality improvement of distribution system with photovoltaic and permanent magnet synchronous generator based renewable energy farm using static synchronous compensator. *Sustain Energy Technol Assess* 35:98–116
- Noureldeen O, Ibrahim AM (2018) Modeling, implementation and performance analysis of a grid-connected photovoltaic/wind hybrid power system. In: *International conference on innovative trends in computer engineering (ITCE)*, pp 296–304
- General Electric (GE) wind turbine. <https://en.wind-turbine-models.com/turbines/656-general-electric-ge-1.5xle>
- Ma T, Cintuglu MH, Mohammed OA (2017) Control of a hybrid AC/DC microgrid involving energy storage and pulsed loads. *IEEE Trans Ind Appl* 53:567–575
- Zhu L, Li Q, Chen M, Cao K, Sun Y (2019) A simplified mathematical model for power output predicting of Building Integrated Photovoltaic under partial shading conditions. *Energy Convers Manag* 180:831–843
- Strand BE (2008) Voltage support in distributed generation by power electronics. M.Sc. Thesis, Dept. Electrical Power Eng., Norwegian University of Science and Technology
- Al-Ogaili AS, Aris IB, Verayah R, Ramasamy A, Marsadek M, Rahmat NA, Hoon Y, Aljanad A, Al-Masri AN (2019) A three-level universal electric vehicle charger based on voltage-oriented control and pulse-width modulation. *Energies* 12:2375
- Althobaiti A, Armstrong M, Elgendy M (2016) Current control of three-phase grid-connected PV inverters using adaptive PR controller. In: *2016 7th International Renewable Energy Congress (IREC)*, pp 1–6
- Laabidi H, Mami A (2015) Grid connected Wind-Photovoltaic hybrid system. In: *5th International Youth Conference on Energy (IYCE)*, pp 1–8
- Kou W, Wei D, Zhang P, Xiao W (2015) A direct phase-coordinates approach to fault ride through of unbalanced faults in

- large-scale photovoltaic power systems. *Electr Power Compon Syst* 43:902–913
29. Hossain MK, Ali MH (2016) Transient stability augmentation of PV/DFIG/SG-based hybrid power system by parallel-resonance bridge fault current limiter. *Electr Power Syst Res* 130:89–102
 30. Nourelddeen O, Ibrahim A (2018) Performance analysis of grid connected PV/Wind Hybrid power system during variations of environmental conditions and load. *Int J Renew Energy Res* 8:208–220
 31. Oskouei AB, Banaei MR, Sabahi M (2016) Hybrid PV/wind system with quinary asymmetric inverter without increasing DC-link number. *Ain Shams Eng J* 7:579–592
 32. Izadbakhsh M, Rezvani A, Gandomkar M (2015) Dynamic response improvement of hybrid system by implementing ANN-GA for fast variation of photovoltaic irradiation and FLC for wind turbine. *Arch Electr Eng* 64:291–314
 33. Alaraifi S, Moawwad A, El Moursi MS, Khadkikar V (2013) Voltage booster schemes for fault ride-through enhancement of variable speed wind turbines. *IEEE Trans Sustain Energy* 4:1071–1081
 34. Tohidi S, Behnam M-I (2016) A comprehensive review of low voltage ride through of doubly fed induction wind generators. *Renew Sustain Energy Rev* 57:412–419
 35. Tohidi S, Tavner P, McMahon R, Oraee H, Zolghadri M, Shao S, Abdi E (2014) Low voltage ride-through of DFIG and brushless DFIG: similarities and differences. *Electr Power Syst Res* 110:64–72
 36. Parida A, Chatterjee D (2016) Model-based loss minimisation scheme for wind solar hybrid generation system using (grid-connected) doubly fed induction generator. *IET Electr Power Appl* 10:548–559
 37. Parida A, Chatterjee D (2016) Cogeneration topology for wind energy conversion system using doubly-fed induction generator. *IET Power Electron* 9:1406–1415
 38. Singh B, Aggarwal SK, Kandpal TC (2010) Performance of wind energy conversion system using a doubly fed induction generator for maximum power point tracking. In: *IEEE Industry Applications Society Annual Meeting (IAS)*, pp 1–7
 39. Chen M, Fan D, Fang H, Zhu Y, Chen P (2017) Control strategy of excitation converter in Doubly-Fed Induction Generator wind power generation system. In: *IEEE Conference on Energy Internet and Energy System Integration (EI2)*, pp 1–5
 40. Parida A, Chatterjee D (2016) An improved control scheme for grid connected doubly fed induction generator considering wind-solar hybrid system. *Int J Electr Power Energy Syst* 77:112–122
 41. Ayodele TR, Jimoh A-GA, Munda J, Agee J (2013) Dynamic response of a wind farm consisting of Doubly-Fed Induction Generators to network disturbance. In: *Simulation and modeling methodologies, technologies and applications*, ed. Springer, pp 131–150
 42. Mohammadi J, Vaez-Zadeh S, Ebrahimzadeh E, Blaabjerg F (2018) Combined control method for grid-side converter of doubly fed induction generator-based wind energy conversion systems. *IET Renew Power Gener* 12:943–952
 43. Singh B, Saha R, Chandra A, Al-Haddad K (2009) Static synchronous compensators (STATCOM): a review. *IET Power Electron* 2:297–324
 44. Yang Y, Blaabjerg F (2013) Low-voltage ride-through capability of a single-stage single-phase photovoltaic system connected to the low-voltage grid. *Int J Photoenergy*. <https://doi.org/10.1155/2013/257487>
 45. Bae Y, Vu T-K, Kim R-Y (2013) Implemental control strategy for grid stabilization of grid-connected PV system based on German grid code in symmetrical low-to-medium voltage network. *IEEE Trans Energy Convers* 28:619–631
 46. Sahoo AK, Murugesan K, Thygarajan T (2006) Modeling and simulation of 48-pulse VSC based STATCOM using simulink's power system blockset. In: *India international conference on power electronics*, pp 303–308
 47. El-Moursi M, Sharaf A (2005) Novel controllers for the 48-pulse VSC STATCOM and SSSC for voltage regulation and reactive power compensation. *IEEE Trans Power Syst* 20:1985–1997
 48. Suresh Y, Panda A (2010) Dynamic performance of statcom under line to ground faults in power system. In: *5th IET international conference on power electronics, machines and drives (PEMD 2010)*, pp 1–6
 49. Rauf AM, Khadkikar V (2015) Integrated photovoltaic and dynamic voltage restorer system configuration. *IEEE Trans Sustain Energy* 6:400–410

Publisher's Note Springer Nature remains neutral with regard to jurisdictional claims in published maps and institutional affiliations.